



# Delineating the Seasonally Modulated Nonlinear Feedback Onto ENSO From Tropical Instability Waves

Aoyun Xue, Fei-Fei Jin, Wenjun Zhang, Julien Boucharel, Sen Zhao, Xinyi Yuan

## ► To cite this version:

Aoyun Xue, Fei-Fei Jin, Wenjun Zhang, Julien Boucharel, Sen Zhao, et al.. Delineating the Seasonally Modulated Nonlinear Feedback Onto ENSO From Tropical Instability Waves. *Geophysical Research Letters*, 2020, 47, 10.1029/2019GL085863 . insu-03671099

HAL Id: insu-03671099

<https://insu.hal.science/insu-03671099>

Submitted on 18 May 2022

**HAL** is a multi-disciplinary open access archive for the deposit and dissemination of scientific research documents, whether they are published or not. The documents may come from teaching and research institutions in France or abroad, or from public or private research centers.

Copyright

L'archive ouverte pluridisciplinaire **HAL**, est destinée au dépôt et à la diffusion de documents scientifiques de niveau recherche, publiés ou non, émanant des établissements d'enseignement et de recherche français ou étrangers, des laboratoires publics ou privés.

# Geophysical Research Letters

## RESEARCH LETTER

10.1029/2019GL085863

### Key Points:

- Nonlinear dynamical heating (NDH) due to tropical instability waves (TIWs) is largely proportional to the amplitude of a simple TIW index
- TIW feedback onto El Niño–Southern Oscillation through TIW-induced NDH is nonlinear and strongly seasonal dependent
- A theoretical derived simple expression for this feedback is in agreement with the deduced result from the reanalysis data

### Supporting Information:

- Supporting Information S1

### Correspondence to:

F.-F. Jin, and W. Zhang, jff@hawaii.edu  
eduzhangwj@nuist.edu.cn

### Citation:

Xue, A., Jin, F.-F., Zhang, W., Boucharel, J., Zhao, S., & Yuan, X. (2020). Delineating the seasonally modulated nonlinear feedback onto ENSO from tropical instability waves. *Geophysical Research Letters*, 47, e2019GL085863. <https://doi.org/10.1029/2019GL085863>

Received 5 NOV 2019

Accepted 8 FEB 2020

Accepted article online 24 MAR 2018

## Delineating the Seasonally Modulated Nonlinear Feedback Onto ENSO From Tropical Instability Waves

Aoyun Xue<sup>1</sup> , Fei-Fei Jin<sup>2</sup> , Wenjun Zhang<sup>1</sup> , Julien Boucharel<sup>3</sup> , Sen Zhao<sup>1,2</sup> , and Xinyi Yuan<sup>1</sup> 

<sup>1</sup>CIC-FEMD/ILCEC, Key Laboratory of Meteorological Disaster of Ministry of Education (KLME), Nanjing University of Information Science and Technology, Nanjing, China, <sup>2</sup>Department of Atmospheric Sciences, SOEST, University of Hawai'i at Mānoa, Honolulu, HI, USA, <sup>3</sup>LEGO, University of Toulouse, CNRS, IRD, CNES, UPS, Toulouse, France

**Abstract** Tropical instability waves (TIWs), the dominant form of eddy variability in the tropics, have a peak period at about 5 weeks and are strongly modulated by both the seasonal cycle and El Niño–Southern Oscillation (ENSO). In this study, we first demonstrated that TIW-induced nonlinear dynamical heating (NDH) is basically proportional to the TIW amplitude depicted by a complex index for TIW. We further delineated that this NDH, capturing the seasonally modulated nonlinear feedback of TIW activity onto ENSO, is well approximated by a theoretical formulation derived analytically from a simple linear stochastic model for the TIW index. The results of this study may be useful for the climate community to evaluate and understand the TIW-ENSO multiscale interaction.

**Plain Language Summary** Tropical instability waves (TIWs) are westward propagating high-frequency waves having a main period about 5 weeks. Their activity is strongly modulated by the cold tongue annual cycle and El Niño–Southern Oscillation (ENSO). At the same time, TIW activity as a whole systematically transports heat meridionally from warm to cold regions, and thus when they are modulated by ENSO, they can have a nonlinear rectification effect on ENSO in return. We find that the TIW-induced rectification effect on ENSO can be related to the amplitude of a simple index that captures the main propagative wavy feature of TIW. This feedback effect prevents the growth of La Niña (El Niño) events by promoting a warming (cooling) through meridional convergence of TIW heat transport. Finally, we introduce a theoretical formulation for TIW-induced effect by adopting a simple linear stochastic model for TIW focused on the complex index for TIW. This validated formulation shall be useful, for instance, for evaluating and understanding the climate model's ability in simulating the TIW-ENSO multiscale interaction.

## 1. Introduction

Tropical instability waves (TIWs) are intraseasonal synoptic wave features that form in the tropical Pacific and Atlantic Oceans, with a wavelength of 1,000–2,000 km and a period of 20–40 days (Legeckis, 1977; Qiao & Weisberg, 1995; Weisberg & Weingartner, 1988). TIWs arise from the combined effect of barotropic instabilities from the meridional shears of the equatorial current system (Cox, 1980; Philander, 1978; Im et al., 2012) and baroclinic instabilities due to the sea surface temperature (SST) meridional gradient in the Eastern Tropical Pacific (Hansen & Paul, 1984; Wilson & Leetmaa, 1988; Yu et al., 1995). Thus, TIW activity is suppressed during the warm phase of the cold tongue when the SST meridional gradient is weakened. Whereas TIW activity is strengthened during the cold phase of the cold tongue due to the sharpened SST meridional gradient (Vialard et al., 2001; Wu & Bowman, 2007; J.-Y. Yu & Liu, 2003).

Some studies pointed that the mixing from TIWs induced by nonlinear eddy heat flux and nonlinear dynamical heating (NDH) (Jin et al., 2003) over the eastern equatorial Pacific (EEP) could partly explain El Niño–Southern Oscillation (ENSO) asymmetry (e.g., An, 2008; Bryden & Brady, 1989; Imada & Kimoto, 2012; Menkes et al., 2006; Swenson & Hansen, 1999; Yu & Liu, 2003). Therefore, TIWs act as an asymmetric negative feedback onto ENSO and influence the cold tongue mean state through rectified nonlinear feedbacks. Specifically, they induce an anomalous cooling during El Niño and warming during La Niña (An, 2008; Jochum & Murtugudde, 2004; Menkes et al., 2006). Previous studies have mentioned that TIW-induced

heat fluxes have a significant contribution to the mixed layer heat budget, comparable to the one from atmospheric heat fluxes (Baturin & Niiler, 1997; Bryden & Brady, 1989). Menkes et al. (2006) estimated the TIW-induced horizontal advection using an ocean general circulation model (GCM), which leads to a warming of 0.84 °C/month in the EEP. Imada and Kimoto (2012) also show, using a high-resolution ocean model, that intensified TIWs during boreal summer/fall increase the tropical eastern Pacific SST due to the warm thermal advection by anomalous currents, with a rate of up to 1 °C/month. Although the TIWs influence on the cold tongue heat budget has been highlighted in previous studies, the coarse spatial and temporal resolutions of observed SST and ocean currents as well as the cold tongue bias in GCMs make it difficult to resolve TIWs and thus quantify their impact accurately (Graham, 2014; Wang & McPhaden, 1999; Wang & Weisberg, 2001).

The main objective of this study is to quantify the nonlinear heat flux convergence feedback from TIWs onto ENSO using observational data as well as to validate a simple theoretical formulation for this feedback derived in Boucharel and Jin (2020) (BJ20, hereafter). To do so, after presenting in section 2 the data sets and TIW indices, we propose in section 3 two different methods to assess TIW amplitude and the associated NDH from a reanalysis product and in situ data. In section 4, we compare these observational estimates of TIW amplitude and associated NDH feedback to a simple analytical formulation that allows disentangling the influence of TIW-induced NDH on ENSO from different timescales. Section 5 summarizes our findings.

## 2. Data and Methodology

### 2.1. Reanalysis and In Situ Products

We utilize the oceanic temperature and currents data from the NCEP Global Ocean Data Assimilation System (GODAS) pentad product (Behringer & Xue, 2004; Saha et al., 2006). GODAS is available over the period 1980–2018 at a  $1/3^\circ \times 1^\circ$  horizontal resolution in the tropics and a 10-m vertical resolution, enough to capture TIW variability. For the calculation of TIW-induced heat flux and NDH, we apply a 10–60 days band-pass Fourier filtering method to the mixed layer averaged ocean temperature and current fields (Lyman et al., 2005; Qiao & Weisberg, 1995; Shinoda et al., 2009). Additionally, we assessed TIW variability using the unfiltered daily ocean temperature measurements at 1-m depth from the TOGA-TAO (Tropical Atmosphere Ocean) array (McPhaden et al., 1998) over the EEP region. The statistical significance is determined based on a two-tailed Student's *t* test.

### 2.2. TIW Indices

A complex TIW index is calculated based on the previous definition by BJ20. In this study, the real part of the TIW index (TIW1) is simply extracted as the equally spaced and weighted (but with alternating signs) summation of unfiltered surface meridional current anomalies ( $v'$ ) averaged in the  $0\text{--}5^\circ\text{N}$  latitudinal band at six referenced points along  $150\text{--}110^\circ\text{W}$  (black dots; Figures 1c and 1d). We used meridional currents anomalies instead of SST anomalies ( $T'$ ) because they have a stronger signature at TIWs timescale. To capture TIWs westward propagation and thus the main TIW period, we define the imaginary part of the TIW index (TIW2) in the same way as TIW1, except the base points are all shifted by a fixed distance representing a  $90^\circ$  zonal phase shift (red dots; Figures 1c and 1d). The complex TIW index is then defined as

$$\text{TIW1} = \sum \pm v'(t, \text{nodes})/n, \quad \text{TIW2} = \sum \pm v'\left(t, \text{nodes} + \frac{l}{4}\right)/n,$$

$$Z = \text{TIW1} + i\text{TIW2},$$

where  $l$  represents the wavelength (in degrees) which is determined from the leading complex empirical orthogonal function mode in supporting information Figure S1 and Text S1, and  $n$  is the number of points. The TIW amplitude is expressed as  $|Z|^2 = \text{TIW1}^2 + \text{TIW2}^2$ .

The lead-lag cross correlation between TIW1 and TIW2 exhibits some interesting features shown in Figure 1 a. The maximum positive correlation appears when TIW2 leads TIW1 by one to two pentads (5–10 days) and the minimum negative correlation when TIW1 leads TIW2 by one to two pentads. The TIWs damping rate (*e*-folding time) can be assessed with the TIW1 autocorrelation (Figure 1a, red line). The power spectra in Figure 1b also exhibit clear peaks corresponding to a main periodicity at 20–40 days for all indices.

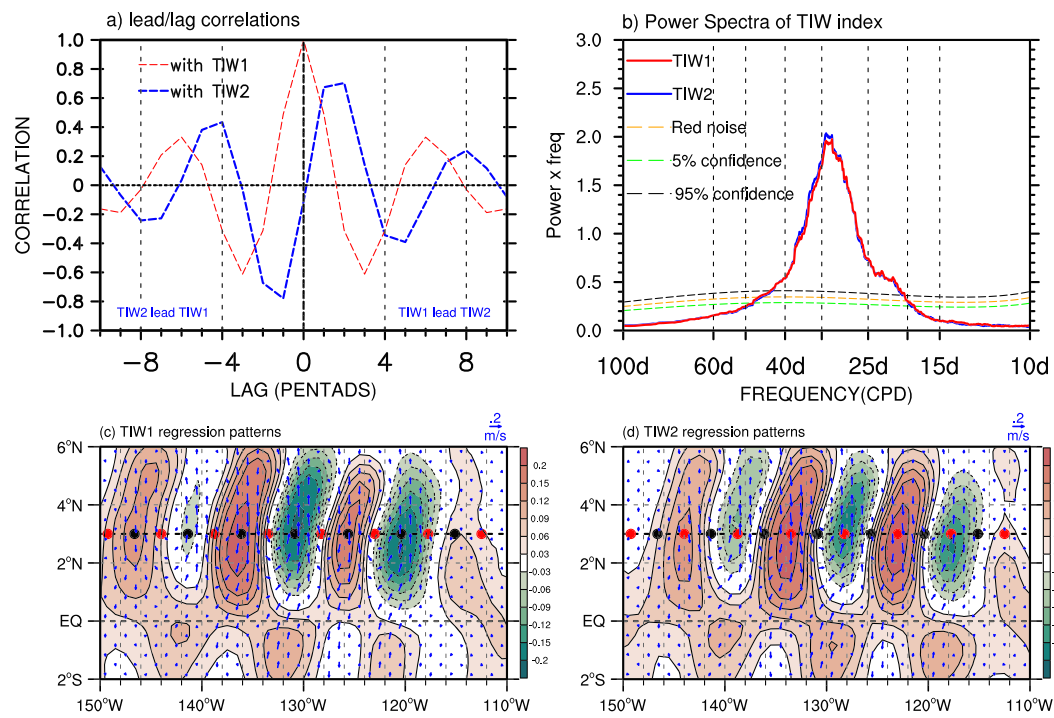


**Figure 1.** (a) Lead/lag correlations between TIW1 and TIW2 (blue line) and TIW1 autocorrelation (red line). (b) Power spectra of the normalized TIW index time series, red (blue) line are for TIW1 (TIW2). The plotting format forces the area under the power curve to be equal in any frequency band to the variance. The dashed orange line is the red-noise spectrum inferred from first-order autoregressive process. The 5% (95%) confidence intervals are shown by the dashed green (black) lines. (c, d) The arrows fields show the regressed spatial patterns of the meridional current anomalies onto the normalized TIW1 and TIW2, respectively. Shadings in (c) and (d) represent the linear regression of the mixed layer averaged ocean temperature anomalies onto the same complex TIW index. All results are statistically significant above the 99% confidence level.

Moreover, the complex TIW index has a high consistency with the principal component time series of the leading complex empirical orthogonal function mode (Figures S1c–S1f), which reveals that the complex TIW index could capture accurately TIWs characteristics.

### 3. TIW-Induced NDH in Different Data Sets

#### 3.1. TIW-Induced NDH in GODAS

Previous studies have demonstrated that TIW activity is mainly modulated by ENSO and the annual cycle, and acts as a negative feedback onto ENSO through TIW-induced NDH (An, 2008). We showed in the supplementary material that the mixed layer contribution of TIW-induced zonal averaged zonal and vertical heat fluxes onto the climate mean state and ENSO is negligible (Figure S3), consistently with previous studies (e.g., Bryden & Brady, 1989; Hansen & Paul, 1984). Thus, we here first to focus on developing a simple method to approximately estimate the TIW-induced nonlinear meridional heat flux and NDH.

The effectiveness of TIWs in generating nonlinear meridional heat flux and NDH can be seen clearly from the TIWs in-phase spatial patterns of the mixed layer oceanic currents (arrows) and temperature (shading) associated with the TIW index as shown in Figures 1c and 1d. They display a series of alternating cyclonic (wave trough) and anticyclonic (wave crest) circulations in the north of the equator. Relatively weak TIW patterns are also found in the south of the equator. The strong spatial coherence between the meridional currents and temperature anomalies fields highlights a potentially strong meridional convergence of equatorward heat flux.

We can reconstruct the meridional current and temperature anomalies from the regressed patterns as follows:

$$\begin{aligned} v' &= \underbrace{\text{TIW1} \times v_r + \text{TIW2} \times v_i}_{\text{term1}} + R_1 \\ T' &= \underbrace{\text{TIW1} \times T_r + \text{TIW2} \times T_i}_{\text{term2}} + R_2, \end{aligned} \quad (1)$$

where  $v_r$  and  $v_i$  in equation (1) represent respectively the real and imaginary parts of the regressed spatial mode of meridional current anomalies onto the complex TIW index. We adopt a similar formulation for  $T_r$  and  $T_i$ .  $R_1$  and  $R_2$  represent the residual terms after removing the regressed part of  $v'$  and  $T'$ , respectively. We can calculate the heat flux based on the reconstructed  $v'$  and  $T'$  fields as follows:

$$v' T' = \underbrace{(\text{term1} \times \text{term2}, 2)}_{\text{reconstructed term}} + \underbrace{R_1 \times \text{term2}}_{\text{cross term1}} + \underbrace{R_2 \times \text{term1}}_{\text{cross term2}} + \underbrace{R_1 \times R_2}_{\text{residual term}}. \quad (2)$$

Since the spatial pattern real and imaginary parts are orthogonal and the meridional current and temperature fields are spatially in-phase, we can obtain the following approximation  $[v_r T_r] \approx [v_i T_i]$  and thus  $[v_r T_r + v_i T_r] \approx 0$  as shown in Figures S4a and S4b. Here, the brackets represent the area average over the TIWs most active region ( $0\text{--}5^\circ\text{N}$ ,  $150\text{--}110^\circ\text{W}$ ). Moreover, the residual term also has high correlation with the reconstructed term ( $R = 0.62$ ) (Figure S4e). This is because the time evolution of the residual parts  $R_1$  and  $R_2$  of TIW activity are in fact also modulated in a similar way as the TIW amplitude. This is a remarkable and allows us approximating the whole nonlinear heat flux using the reconstructed  $v'$  and  $T'$  fields as follows:

$$-\tilde{[v' T']} (t) = -\sigma (\text{TIW1}^2 + \text{TIW2}^2) * [v_r T_r]. \quad (3)$$

Here the above tilde refers to the 3 month running average.  $\sigma$  can be obtained as the regression coefficient of the reconstructed heat flux on the TIW index ( $\sigma = 5.37\text{E+6}$ ). We further approximate  $\frac{\partial \tilde{[v' T']}}{\partial y}$  as  $\frac{\tilde{[v' T']}}{L}$ . Hence, TIW-induced NDH feedback onto ENSO can be formulated as

$$\text{NDH} = -\frac{\partial \tilde{[v' T']}}{\partial y} = -\frac{\tilde{[v' T']}}{L} \approx \frac{\sigma}{L} \times \tilde{|Z|^2} \times [v_r T_r] = -I_\sigma \times \tilde{|Z|^2} \times [v_r T_r], \quad (4)$$

$L$  is the TIWs meridional effective scale and reflects the width of the spatial region used to average these quantities.  $I_\sigma$  ( $I_\sigma = 16.80$ ) the scaling factor and  $|Z|^2$  is the TIW amplitude.

Figure 2a shows the interannual variation of the reconstructed TIW-induced NDH from the complex TIW index and the observed TIW-induced NDH in the form of  $-\frac{\tilde{[v' T']}}{L}$ . Both time series are highly correlated ( $R = 0.87$ ), again confirming the ability of our simple index to capture the modulation of TIW activity, and exhibit a strong positive asymmetry, with values of  $0.4\text{--}0.6^\circ\text{C/month}$  over the EEP during La Niña and close to zero during El Niño. To further illustrate the asymmetry of the NDH feedback onto ENSO, the relationship between the Niño3.4 index and the interannual part of the reconstructed TIW-induced NDH is shown in Figure 2b. Consistently with previous studies (An, 2008; BJ20), this relationship is found to be highly nonlinear with strong/weak NDH values during La Niña/El Niño. Thus, the TIW-induced NDH is modulated by ENSO and acts as asymmetric feedback onto ENSO. Interestingly, the NDH power spectrum (Figure 2c) also exhibits significant peaks not only at the ENSO frequency  $f$  but also at frequencies  $1+f$  and mostly  $1-f$  ( $1$  being the annual cycle frequency). These frequencies emerge from the nonlinear interaction between ENSO and the annual cycle of SST and mixed layer circulation in the EEP, which reflects a similar combination tone (C tone) as the one described by Stuecker et al. (2013, 2015, 2017) but with a different seasonality as TIWs are more active during the boreal summer. This C tone implies that ENSO-TIW multiscale interaction will contribute to generate a combination tone in ENSO, a subject beyond the scope of this study.

To illustrate and quantify the seasonally modulated influence of TIW-induced NDH onto ENSO, we break down, in Figures 2d and 2e, the Niño3.4/NDH relationship into active (August–December) and inactive (February–June) seasons of TIW activity (Figures S2c and S2d). The nonlinear feedback between ENSO and TIW-induced NDH is strongly enhanced during boreal summer (Figure 2d) and reduced during

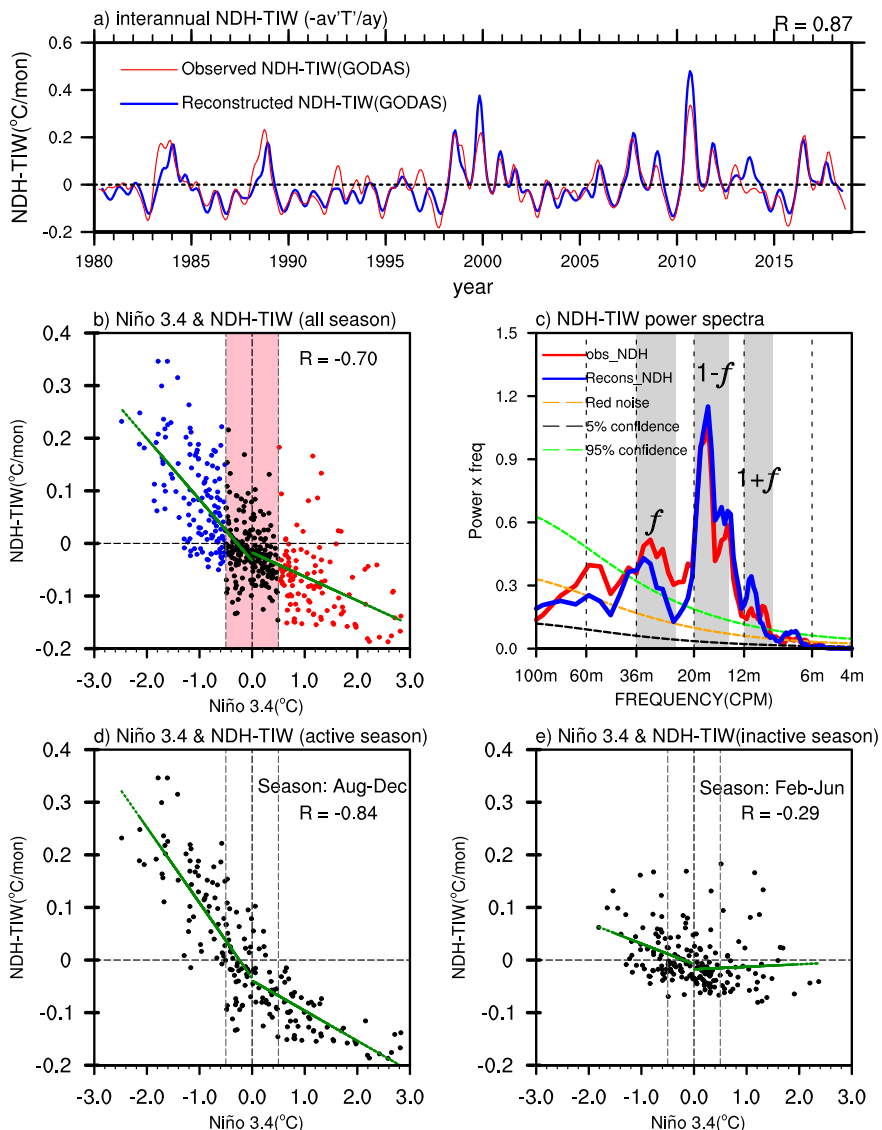


**Figure 2.** (a) Interannual part of the 3 month running mean and area-averaged time series of the observed TIW-induced NDH (red line) and reconstructed NDH with the TIW index (blue line). Correlations are statistically significant above the 99% confidence level; (b) scatterplot of the relationship between Niño3.4 index and reconstructed TIW-induced NDH. Red (blue) dots are used when  $\text{Niño } 3.4 > 0.5$  ( $\text{Niño } 3.4 < -0.5$ ). Black dots in the pink area represents ENSO neutral condition (i.e.,  $-0.5 < \text{Niño } 3.4 < 0.5$ ); the green lines show the slopes of the linear regressions associated with both positive and negative Niño3.4 values. (c) Power spectra of the normalized TIW-induced NDH time series. The plotting format is the same as in Figure 1b. The interannual ENSO forcing frequency  $f$ , as well as the near-annual ( $1 \pm f$ ) combination tones are labeled in the gray areas. CPM stands for cycle per month; (d, e) the Niño3.4 index and TIW-induced NDH scatterplots during TIW active (August–December), respectively inactive (February–June) seasons. The green lines are the same as for Figure 2d.

winter (Figure 2e), which suggests that the TIW activity is seasonally modulated by the C tone variability, then in turn affecting ENSO through rectification processes as explained in text S2.

### 3.2. TIW-Induced NDH in TAO

Most current GCMs and reanalysis products are not able to accurately resolve TIWs features due to their too coarse spatiotemporal resolution and biases in simulating the SST and circulation in the EEP (e.g., Graham, 2014; Tatebe & Hasumi, 2010). Thus, one must take cautiously the results from the previous section about the (i) the evaluation of the TIW-induced NDH and (ii) its relationship with ENSO. To address this issue,

we propose a method to assess TIW activity and associated NDH from the TAO array data set, which provides sparse but zonally aligned direct in situ measurements.

We use daily SST time series (1980–2016) from three mooring locations ( $2^{\circ}\text{N}$ ,  $110^{\circ}\text{W}$ ;  $2^{\circ}\text{N}$ ,  $125^{\circ}\text{W}$  and  $2^{\circ}\text{N}$ ,  $150^{\circ}\text{W}$ ) to reassess the previous evaluation of TIW-induced NDH from the GODAS reanalysis product. Since TIWs exhibit spatial and temporal coherent features, we can use the wave space–time equivalence to retrieve the wave characteristics from these fixed locations along the EEP. Instead of shifting longitudinally the locations of certain points of the GODAS gridded product based on TIWs wavelength to assess TIWs propagating features (cf. section 2), we now shift in time (based on TIWs period) the SST data at the fixed mooring locations to reconstruct the TIWs propagation. By considering that TIWs are equally spaced and weighted in propagation, we can write for each of the three moorings the following equations to approximate TIW1/TIW2:

$$\text{TIW1} = T_1(t-t1) - T_1(t+t1') + T_2(t-t2) - T_2(t+t2') + T_3(t-t3) - T_2(t+t3'), \quad (5a)$$

$$\text{TIW2} = T_1(t-t01) - T_1(t+t01') + T_2(t-t02) - T_2(t+t02') + T_3(t-t03) - T_2(t+t03'), \quad (5b)$$

where the TIW index consists of three pairs of SSTA differences between two adjacent interpolated points (same as the six fixed points in Figures 1c and 1d) from the three observed locations ( $T_1$ ,  $T_2$ ,  $T_3$ ). This allows removing any trend, low frequency variability as well as the annual cycle.  $t1$ ,  $t2$ ,  $t3$  ( $t01$ ,  $t02$ ,  $t03$ ) and  $t1'$ ,  $t2'$ ,  $t3'$  ( $t01'$ ,  $t02'$ ,  $t03'$ ) are the lead/lag time between the fixed black (red) interpolated points and the nearest locations calculated using the TIWs wave speed ( $c$ ) and intermooring distance ( $l$ ) (i.e.,  $t = \frac{l}{c}$ ). We can now evaluate the observed TIW amplitude and NDH from the TAO data set.

Figure 3 compares TIW1 and TIW2 characteristics as inferred from GODAS and TAO. TIWs extracted from both data sets exhibit a similar period, damping rate (Figures 3a and S5b) and spectra of TIW amplitude (Figure 3b). There is a strong correlation between the GODAS and TAO 3 month smoothed TIW amplitude ( $R = 0.81$ ; Figure S5a) but the amplitude is significantly stronger in TAO than GODAS. Both their power spectra indicate a strong dominance of the C tone variability (Figure 3b). We also observed the TIW-induced seasonally modulated asymmetric NDH feedback onto ENSO in the TAO data set (Figure S5c), with values up to  $0.8^{\circ}\text{C/month}$  during La Niña and approximately  $-0.4^{\circ}\text{C/month}$  during El Niño events, which is comparable to other heat flux terms (such as the zonal advective and thermocline feedbacks) in the mixed layer heat budget as Figure S6 shows. The interannual variability of TIW-induced NDH is in good agreement between TAO and GODAS ( $R = 0.76$ ; Figure 3c), although the amplitude of the nonlinear meridional heat flux is nearly three times larger in TAO. This again highlights the underestimation of TIW amplitude and NDH in GODAS.

Interestingly, the method presented here can serve to assess and potentially correct biases in the models' representation of TIWs. For instance, we can use the comparison between the TIWs inferred from in situ data and from the reanalysis product to quantify the rate of underestimation of TIW amplitude in the model. In this case, by calculating the ratio of TIW variance between GODAS and TAO, we find a rate of TIW amplitude underestimation in GODAS of  $\gamma = 3.10$ . See supplementary material (Figure S7) for more details.

#### 4. A Simple Analytical Formulation of TIW-Induced NDH

Recently, BJ20 have introduced a stochastically forced linear model for TIW amplitude with its damping rate modulated by the EEP annual cycle and ENSO. It is an extension of the model by Hasselmann (1976) and Frankignoul and Hasselmann (1977) and can be written as follows:

$$\frac{dZ}{dt} = \left[ -\left( \gamma_0 + \frac{2i\pi}{T} \right) + \left( \gamma_A \cos \frac{2\pi(t-\varphi)}{T_A} \right) + (\gamma_N \text{Ni}\tilde{\text{o}}3.4(t)) + (\gamma_{N^3} \text{Ni}\tilde{\text{o}}3.4(t)^3) \right] Z + \omega(t), \quad (6)$$

where  $Z = \text{TIW1} + i\text{TIW2}$ ;  $dZ/dt$  is the TIW amplitude tendency,  $\omega(t)$  is a white noise forcing and  $\text{Ni}\tilde{\text{o}}3.4$  the ENSO forcing.  $T = 36$  days and  $T_A = 365$  days are respectively the TIW and annual cycle periods.  $\gamma_0$  is the mean damping rate and  $\gamma_A$  and  $\gamma_N$  are the annual and interannual modulation of TIWs damping rate by the cold tongue annual cycle and ENSO respectively. The phase for the annual damping rate  $\varphi$  is so chosen such that TIW amplitude reaches a maximum in boreal Summer and a minimum in Spring ( $\varphi=120\text{d}$ ). To

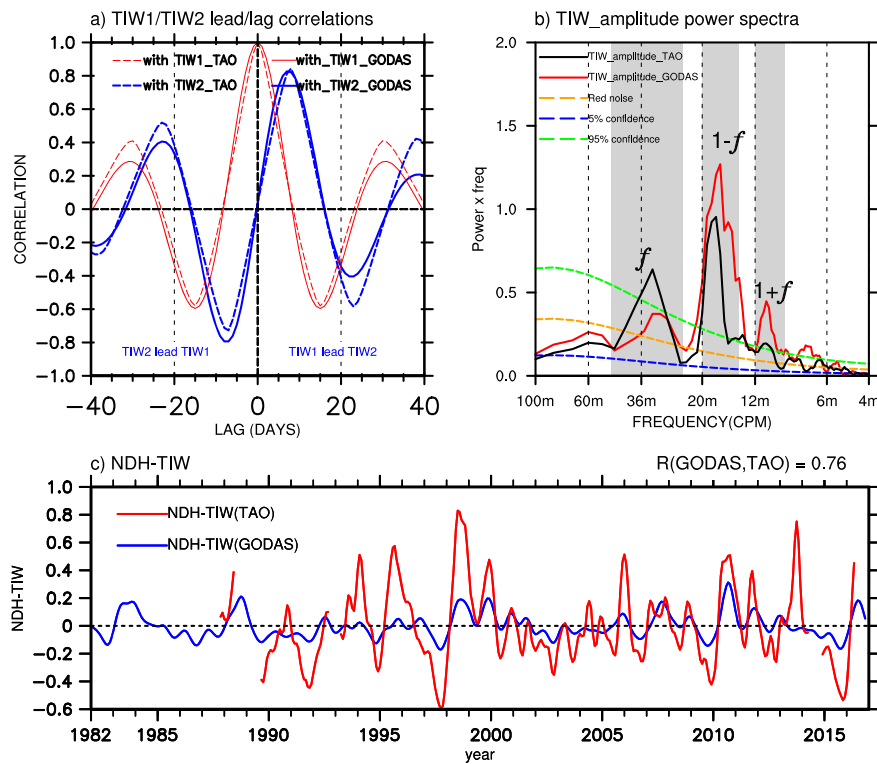


**Figure 3.** (a) Lead/lag correlations between TIW1 and TIW2 extracted from GODAS (blue solid line) and TAO (blue dashed line) and TIW1 autocorrelation from GODAS (red solid line) and TAO (red dashed line). (b) Power spectra of TIW amplitude inferred from GODAS (red line), respectively from TAO (black line). The plotting format is the same as in Figure 1b; (c) 3 month running average and area-averaged interannual time series of TIW-induced NDH calculated from TAO (red line) and from GODAS (blue line).

account for the ENSO asymmetrical feedback on TIW amplitude, the nonlinear effect  $\gamma_N^3 \tilde{N}i\tilde{n}o3.4$  is additionally included in the damping rate of the TIW model. As long as  $|\gamma_A/\gamma_0| < 1$ ,  $|\gamma_N/\gamma_0| < 1$  and  $|\gamma_N^3/\gamma_0| < 1$ , the solution of the TIW amplitude can be analytically derived. The details on how to estimate the parameters and how to approximate the analytical solution of the slow variability of TIW amplitude (i.e.,  $|Z|^2$ ) can be found in BJ20. To better account for the dependance of the interannual modulation of TIWs growth rate on the baroclinic instability due to the strong meridional gradient of ocean temperature, we replace Niño3.4 by a new index NiñoD. It is calculated as the meridional difference between the subtropical northeastern Pacific ( $3\text{--}8^\circ\text{N}$ ,  $150\text{--}110^\circ\text{W}$ ) and the EEP ( $3^\circ\text{S}$  to  $3^\circ\text{N}$ ,  $150\text{--}110^\circ\text{W}$ ) SST anomalies. Following BJ20, the modified analytical formulation of the seasonally dependent TIW-induced NDH feedback onto ENSO can be written as follows:

$$\begin{aligned} NDH_{TIW} \approx K \left\{ \underbrace{\frac{\gamma_N}{\gamma_0} \tilde{N}i\tilde{n}oD(t)}_{term1} + \underbrace{\frac{\gamma_N^3}{\gamma_0} \tilde{N}i\tilde{n}oD(t)^3}_{term2} + \underbrace{2 \frac{\gamma_A \gamma_N}{\gamma_0^2} \cos\left(\frac{2\pi(t-\varphi)}{T_A}\right) \times \tilde{N}i\tilde{n}oD(t)}_{term3} + \underbrace{\left(\frac{\gamma_N}{\gamma_0}\right)^2 \tilde{N}i\tilde{n}oD(t)^2}_{term4} \right. \\ \left. + \underbrace{\left(\frac{\gamma_N^3}{\gamma_0}\right) 2 \tilde{N}i\tilde{n}oD(t)^6}_{term5} + \underbrace{(2 \frac{\gamma_A \gamma_N^3}{\gamma_0^2} \cos\left(\frac{2\pi(t-\varphi)}{T_A}\right) \times \tilde{N}i\tilde{n}oD(t)^3)}_{term6} + \underbrace{2 \frac{\gamma_A \gamma_N^3}{\gamma_0^2} \tilde{N}i\tilde{n}oD(t)^4}_{term7} \right\}, \quad (7) \end{aligned}$$

where  $K$  is a constant, which can be explicitly formulated as  $K = \frac{\overline{v' T'}}{L}$ .  $\overline{v' T'}$  represents the observed meridional heat flux climatological average and is estimated as the product of heat flux from GODAS by underestimation rate  $\gamma$ .  $L$  is the meridional scale of TIWs effectiveness (cf. section 3.1). With the proper normalization of

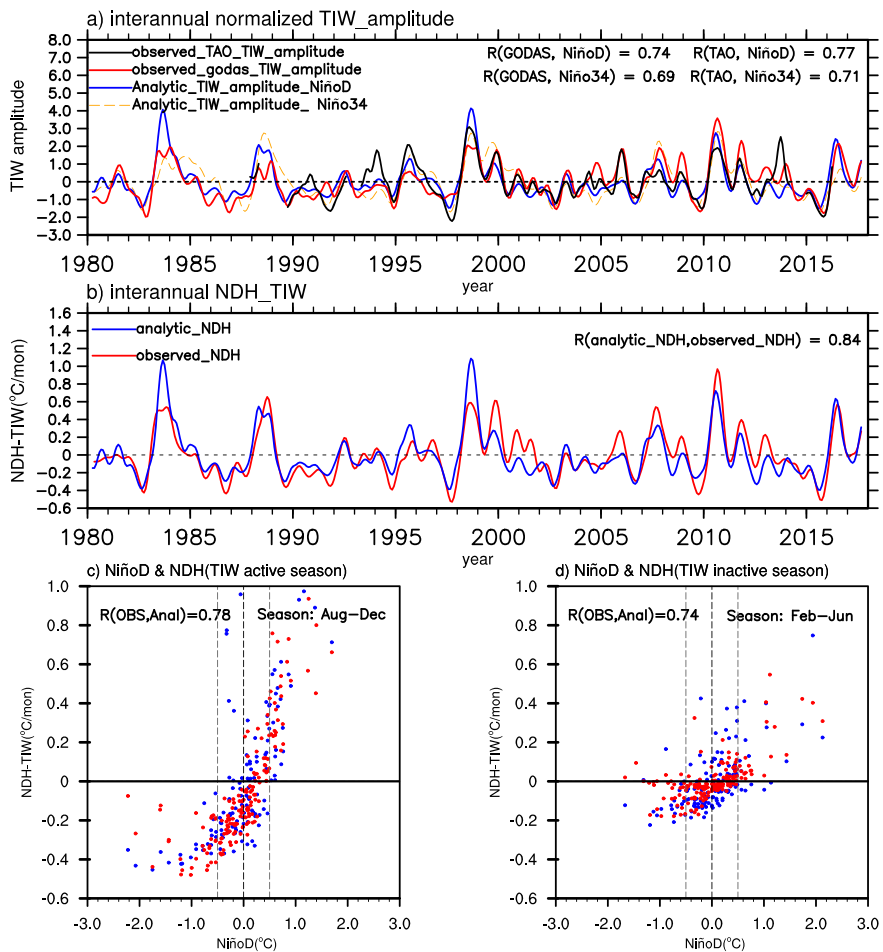


**Figure 4.** (a) Three month running mean of the TIW amplitude interannual variability from TAO (black solid line), GODAS (red line), the model's analytical solution with NiñoD (blue line), and Niño3.4 index (orange dashed line); (b) 3 month running mean of TIW-induced NDH interannual variability from TAO (black line) and the model's analytical solution with NiñoD index (black line). Relationships between NiñoD index and TIW-induced NDH during TIW active (c) and inactive (d) seasons. Red dots are for the observed TIW-induced NDH and blue dots for the theoretical TIW-induced NDH. Correlations are included in the top left corner of each panel.

TIWs,  $NDH_{TIW}$  has therefore the same unit as  $K$  ( $^{\circ}\text{C}/\text{month}$ ). The terms on the right-hand side of equation (7) exhibit a dominant variability at frequencies  $f$ ,  $3f$ ,  $1 \pm f$ ,  $2f$ ,  $6f$ ,  $1 \pm 3f$  and  $4f$ , respectively, which arise from ENSO, the annual cycle, C tone, and higher order nonlinearity in the interannual modulation of TIWs damping rate. We thus expect the TIW-induced NDH feedback onto ENSO nonlinearly with a strong seasonal modulation, a subject beyond the paper but certainly worthy of future investigations.

We first compare the interannual modulation of TIW amplitude as inferred from GODAS, TAO and the analytical approximations. Note that the TIW amplitude in GODAS has been rescaled by the underestimation rate estimated in section 3.2. For the analytical solution, we use the model's original formulation with Niño3.4 and NiñoD. Results show a strong agreement between TIW amplitude inferred from both data sets and formulations of the analytical solution (correlations higher than 0.60; Figure 4a). The modified formulation with NiñoD leads to increased correlations, because of the more explicit assessment of the EEP meridional baroclinic instability.

In Figure 4b, we compare the TIW-induced NDH inferred from TAO and the analytical solution (i.e., equation (7)). Their high correlation ( $R = 0.84$ ) illustrates the success of this analytical framework in assessing the TIWs contribution to ENSO asymmetry. This simple theoretical model also captures the

seasonal modulation of the NDH feedback onto ENSO (Figures 4c, 4d, and S8). Our formulation of this nonlinear feedback may be utilized to understand the influence of ENSO-TIW interactions on ENSO complexity and to diagnose the performance of climate models in simulating the TIW and ENSO interaction.

## 5. Conclusions and Discussions

This paper presents simple tools to assess and quantify the effect of TIWs onto ENSO through the NDH feedback. Following BJ20, we use a simple set of base points, equally spaced according to the typical TIW wavelength, to formulate a complex index of TIW activity. Utilizing TIWs spatiotemporal coherency, we extend this simple way of extracting TIWs from any gridded products, in that case the GODAS reanalysis, to sparsely spaced data set such as TAO in situ moorings. The evaluation and comparison of TIWs features from these two data sets reveal a similar modulation by ENSO but, unsurprisingly a significant underestimation of TIWs variance in GODAS by about a factor  $\sim 3$  compared to in situ measurements.

Secondly, based on these simple characterizations of TIWs, we introduced a method to infer the TIW-induced NDH from the TIW amplitude. Results show that the area-averaged TIW-induced NDH is directly proportional to the amplitude of the simple TIW index. Moreover, the TIW-induced NDH acts as a seasonally modulated nonlinear feedback onto ENSO. This feedback, stronger in boreal summer and fall, prevents the growth of La Niña (El Niño) events by promoting a warming (cooling) of the EEP by up to  $0.8^{\circ}\text{C}/\text{month}$  ( $0.4^{\circ}\text{C}/\text{month}$ ). Thus, our simple TIW index can be used as a straightforward quantification of the effect of TIW activity onto ENSO.

Finally, we modified the analytical formulation of the TIW-induced NDH proposed by BJ20 to account more explicitly for the interannual modulation of TIWs growth rate due to the meridional baroclinic instability. The analytical formulation of TIW-induced NDH is in very good agreement with estimations from observational data. The simple tools presented in this study may be useful for the climate community to evaluate the rectification effects of high-frequency climate transients onto the low frequency climate variability, which may ultimately lead to improve ENSO performance in GCMs and prediction skills of seasonal climate forecasts.

## Acknowledgments

This work is supported by the National Key Research and Development Program (2018YFC1506002) and the National Nature Science Foundation of China (41675073). F. F. J. was supported by the U.S. National Science Foundation (AGS-1813611) and Department of Energy (DE-SC0005110). J. B. is funded by the French Agence Nationale de la Recherche project MOPGA “Trocodyn” (ANR-17-MP04-0018) and the Région Occitanie. GODAS data are available at <https://cfs.ncep.noaa.gov/cfs/godas/pentad/>, TAO data from TAO Project Office of NOAA/PML is downloaded online (from <http://www.pmel.noaa.gov/tao/jdisplay/>).

## References

- An, S.-I. (2008). Interannual variations of the tropical ocean instability wave and ENSO. *Journal of Climate*, 21(15), 3680–3686. <https://doi.org/10.1175/2008JCLI1701.1>
- Baturin, N. G., & Niiler, P. P. (1997). Effects of instability waves in the mixed layer of the equatorial Pacific. *Journal of Geophysical Research, Oceans*, 102(C13), 27,771–27,793. <https://doi.org/10.1029/97JC02455>
- Behringer, D., & Y. Xue (2004). Evaluation of the global ocean data assimilation system at NCEP: The Pacific Ocean, paper presented at Eighth Symposium on Integrated Observing and Assimilation Systems for Atmosphere, Ocean, and Land Surface, AMS 84th Annual Meeting, Amer. Meteor. Soc., Seattle, Wash.
- Boucharel, J., & Jin, F.-F. (2020). A simple theory for the modulation of tropical instability waves by ENSO and the annual cycle. *Tellus A: Dynamic Meteorology and Oceanography*, 72(1), 1–14. <https://doi.org/10.1080/16000870.2019.1700087>
- Bryden, H. L., & Brady, E. C. (1989). Eddy momentum and heat fluxes and their effects on the circulation of the equatorial Pacific Ocean. *Journal of Marine Research*, 47(1), 55–79. <https://doi.org/10.1357/002224089785076389>
- Cox, M. D. (1980). Generation and Propagation of 30-Day Waves in a Numerical Model of the Pacific. *Journal of Physical Oceanography*, 10(8), 1168–1186. [https://doi.org/10.1175/1520-0485\(1980\)010<1168:GAPODW>2.0.CO;2](https://doi.org/10.1175/1520-0485(1980)010<1168:GAPODW>2.0.CO;2)
- Frankignoul, C., & Hasselmann, K. (1977). Stochastic climate models, Part II Application to sea-surface temperature anomalies and thermocline variability. *Tellus*, 29(4), 289–305. <https://doi.org/10.1111/j.2153-3490.1977.tb00740.x>
- Graham, T. (2014). The importance of eddy permitting model resolution for simulation of the heat budget of tropical instability waves. *Ocean Modelling*, 79, 21–32. <https://doi.org/10.1016/j.ocemod.2014.04.005>
- Hansen, D. V., & Paul, C. A. (1984). Genesis and effects of long waves in the equatorial Pacific. *Journal of Geophysical Research*, 89(C6), 10,431. <https://doi.org/10.1029/JC089iC06p10431>
- Hasselmann, K. (1976). Stochastic climate models Part I. Theory. *Tellus*, 28(6), 473–485. <https://doi.org/10.1111/j.2153-3490.1976.tb00696.x>
- Im, S.-H., An, S.-I., Lengaigne, M., & Noh, Y. (2012). Seasonality of tropical instability waves and its feedback to the seasonal cycle in the tropical eastern Pacific. *Scientific World Journal*, 2012, 1–11. <https://doi.org/10.1100/2012/612048>
- Imada, Y., & Kimoto, M. (2012). Parameterization of tropical instability waves and examination of their impact on ENSO characteristics. *Journal of Climate*, 25(13), 4568–4581. <https://doi.org/10.1175/JCLI-D-11-00233>
- Jin, F.-F., An, S.-I., Timmermann, A., & Zhao, J. (2003). Strong El Niño events and nonlinear dynamical heating. *Geophysical Research Letters*, 30(3), 1120. <https://doi.org/10.1029/2002GL016356>
- Jochum, M., & Murtaghuddé, R. (2004). Internal variability of the tropical Pacific Ocean. *Geophysical Research Letters*, 31, L14309. <https://doi.org/10.1029/2004GL020488>
- Legeckis, R. (1977). Long waves in the eastern equatorial Pacific Ocean: A view from a geostationary satellite. *Science*, 197(4309), 1179–1181. <https://doi.org/10.1126/science.197.4309.1179>

- Lyman, J. M., Chelton, D. B., deSzoeke, R. A., & Samelson, R. M. (2005). Tropical instability waves as a resonance between equatorial Rossby waves\*. *Journal of Physical Oceanography*, 35(2), 232–254. <https://doi.org/10.1175/JPO-2668.1>
- McPhaden, M. J., Busalacchi, A. J., Cheney, R., Donguy, J.-R., Gage, K. S., Halpern, D., et al. (1998). The Tropical Ocean-Global Atmosphere observing system: A decade of progress. *Journal of Geophysical Research, Oceans*, 103(C7), 14,169–14,240. <https://doi.org/10.1029/97JC02906>
- Menkes, C. E. R., Vialard, J. G., Kennan, S. C., Boulanger, J.-P., & Madec, G. V. (2006). A modeling study of the impact of tropical instability waves on the heat budget of the eastern equatorial Pacific. *Journal of Physical Oceanography*, 36(5), 847–865. <https://doi.org/10.1175/JPO2904.1>
- Philander, S. G. H. (1978). Instabilities of zonal equatorial currents, 2. *Journal of Geophysical Research: Oceans*, 83(C7), 3679–3682. <https://doi.org/10.1029/JC083iC07p03679>
- Qiao, L., & Weisberg, R. H. (1995). Tropical instability wave kinematics: Observations from the Tropical Instability Wave Experiment. *Journal of Geophysical Research*, 100(C5), 8677. <https://doi.org/10.1029/95JC00305>
- Saha, S., Nadiga, S., Thiaw, C., Wang, J., Wang, W., Zhang, Q., et al. (2006). The NCEP Climate Forecast System. *Journal of Climate*, 19(15), 3483–3517. <https://doi.org/10.1175/JCLI3812.1>
- Shinoda, T., Kiladis, G. N., & Roundy, P. E. (2009). Statistical representation of equatorial waves and tropical instability waves in the Pacific Ocean. *Atmospheric Research*, 94(1), 37–44. <https://doi.org/10.1016/j.atmosres.2008.06.002>
- Stuecker, M. F., Jin, F.-F., & Timmermann, A. (2015). El Niño–Southern Oscillation frequency cascade. *Proceedings of the National Academy of Sciences*, 112(44), 13,490–13,495. <https://doi.org/10.1073/pnas.1508622112>
- Stuecker, M. F., Timmermann, A., Jin, F.-F., Chikamoto, Y., Zhang, W., Wittenberg, A. T., et al. (2017). Revisiting ENSO/Indian Ocean dipole phase relationships: Revisiting ENSO/IOD phase relationships. *Geophysical Research Letters*, 44, 2481–2492. <https://doi.org/10.1002/2016GL072308>
- Stuecker, M. F., Timmermann, A., Jin, F.-F., McGregor, S., & Ren, H.-L. (2013). A combination mode of the annual cycle and the El Niño/Southern Oscillation. *Nature Geoscience*, 6(7), 540–544. <https://doi.org/10.1038/ngeo1826>
- Swenson, M. S., & Hansen, D. V. (1999). Tropical Pacific Ocean mixed layer heat budget: The Pacific cold tongue. *Journal of Physical Oceanography*, 29(1), 69–81. [https://doi.org/10.1175/1520-0485\(1999\)029<069:TPOMLH>2.0.CO;2](https://doi.org/10.1175/1520-0485(1999)029<069:TPOMLH>2.0.CO;2)
- Tatebe, H., & Hasumi, H. (2010). Formation mechanism of the Pacific equatorial thermocline revealed by a general circulation model with a high accuracy tracer advection scheme. *Ocean Modelling*, 35(3), 245–252. <https://doi.org/10.1016/j.ocemod.2010.07.011>
- Vialard, J., Menkes, C., Boulanger, J.-P., Delecluse, P., Guilyardi, E., McPhaden, M. J., & Madec, G. (2001). A model study of oceanic mechanisms affecting equatorial Pacific sea surface temperature during the 1997–98 El Niño. *Journal of Physical Oceanography*, 31(7), 1649–1675. [https://doi.org/10.1175/1520-0485\(2001\)031<1649:AMSOOM>2.0.CO;2](https://doi.org/10.1175/1520-0485(2001)031<1649:AMSOOM>2.0.CO;2)
- Wang, C., & Weisberg, R. H. (2001). Ocean circulation influences on sea surface temperature in the equatorial central Pacific. *Journal of Geophysical Research, Oceans*, 106(C9), 19,515–19,526. <https://doi.org/10.1029/2000JC000242>
- Wang, W., & McPhaden, M. J. (1999). The surface-layer heat balance in the equatorial Pacific Ocean. Part I: Mean seasonal cycle\*. *Journal of Physical Oceanography*, 29(8), 1812–1831. [https://doi.org/10.1175/1520-0485\(1999\)029<1812:TSLHBI>2.0.CO;2](https://doi.org/10.1175/1520-0485(1999)029<1812:TSLHBI>2.0.CO;2)
- Weisberg, R. H., & Weingartner, T. J. (1988). Instability waves in the equatorial Atlantic Ocean. *Journal of Physical Oceanography*, 18(11), 1641–1657. [https://doi.org/10.1175/1520-0485\(1988\)018<1641:IWATEA>2.0.CO;2](https://doi.org/10.1175/1520-0485(1988)018<1641:IWATEA>2.0.CO;2)
- Wilson, D., & Leetmaa, A. (1988). Acoustic Doppler current profiling in the equatorial Pacific in 1984. *Journal of Geophysical Research*, 93(C11), 13,947. <https://doi.org/10.1029/JC093iC11p13947>
- Wu, Q., & Bowman, K. P. (2007). Interannual variations of tropical instability waves observed by the Tropical Rainfall Measuring Mission. *Geophysical Research Letters*, 34, L09701. <https://doi.org/10.1029/2007GL029719>
- Yu, J.-Y., & Liu, W. T. (2003). A linear relationship between ENSO intensity and tropical instability wave activity in the eastern Pacific Ocean. *Geophysical Research Letters*, 30(14), 1735. <https://doi.org/10.1029/2003GL017176>
- Yu, Z., McCreary, J. P., & Proehl, J. A. (1995). Meridional asymmetry and energetics of tropical instability waves. *Journal of Physical Oceanography*, 25(12), 2997–3007. [https://doi.org/10.1175/1520-0485\(1995\)025<2997:MAAEOT>2.0.CO;2](https://doi.org/10.1175/1520-0485(1995)025<2997:MAAEOT>2.0.CO;2)
- Philander, S. G. H. (1978). Instabilities of zonal equatorial currents, 2. *Journal of Geophysical Research*, 83(C7), 3679–3682. <https://doi.org/10.1029/JC083iC07p03679>